J. LIU[1],✉
U.A. GLASMACHER[2]
M. LANG[3],*
C. TRAUTMANN[3]
K.-O. VOSS[3]
R. NEUMANN[3]
G.A. WAGNER[4]
R. MILETICH[5]

Raman spectroscopy of apatite irradiated with swift heavy ions with and without simultaneous exertion of high pressure

[1] Institute of Modern Physics (IMP), Chinese Academy of Sciences, Lanzhou 730000, P.R. China
[2] Geologisch–Paläontologisches Institut (GPI), Ruprecht-Karls-Universität, Heidelberg, Germany
[3] Gesellschaft für Schwerionenforschung (GSI), Darmstadt, Germany
[4] Max-Planck-Institut für Kernphysik (MPI), Heidelberg, Germany
[5] Mineralogisches Institut (MI), Ruprecht-Karls-Universität, Heidelberg, Germany

ABSTRACT Durango apatite was irradiated with energetic U ions of 2.64 GeV and Kr ions of 2.1 GeV, with and without simultaneous exposure to a pressure of 10.5 GPa. Analysis by confocal Raman spectroscopy gives evidence of vibrational changes being marginal for fluences below 5×10^{11} ions/cm^2 but becoming dominant when increasing the fluence to 8×10^{12} ions/cm^2. Samples irradiated with U ions experience severe strain resulting in crystal cracking and finally breakage at high fluences. These radiation effects are directly linked to the formation of amorphous tracks and the fraction of amorphized material increasing with fluence. Raman spectroscopy of pressurized irradiated samples shows small shifts of the band positions with decreasing pressure but without a significant change of the Grüneisen parameter. Compared to irradiations at ambient conditions, the Raman spectra of apatite irradiated at 10.5 GPa exhibit fewer modifications, suggesting a higher radiation stability of the lattice by the pressure applied.

PACS 61.80.Jh; 62.50.+p; 07.35.+k

1 Introduction

Spontaneous fission of ^{238}U in natural minerals leads to a continuous production of particle tracks on a geological time scale and can be used to calculate the time that elapsed since the onset of track accumulation. Durango apatite, containing trace amounts of uranium isotopes, has been employed as an age-dating standard in fission-track laboratories all over the world [1, 2]. Additionally, materials belonging to the class of apatites have been studied as nuclear-waste containment matrices due to their crystal-chemical adaptation, non-stoichiometry, and ability of increasing the density of cation acceptor sites [3]. In these cases, apatite materials are exposed to radiation environments. Since energetic heavy ions from an accelerator produce damage trails similar to fission tracks, they are a suitable tool to mimic fission tracks in minerals under pressure and temperature conditions similar to those occurring in nature. Based on this premise, we chose Durango apatite from Mexico for studies involving heavy-ion irradiation and high pressure.

In previous studies of natural apatite, radiation damage and thermal annealing effects were quantified by investigating ion track damage with channeling Rutherford backscattering spectrometry (CRBS) [4] and transmission electron microscopy (TEM) [5]. Using TEM, the average widths of fission tracks were found to be 9 nm parallel and 5 nm perpendicular to the crystal c axis, respectively [6]. The radius of ion tracks generally increases with increasing electronic energy loss (dE/dx) of the ions. For tracks produced with U ions ($dE/dx = 17.5$ keV/nm) a mean diameter of about 10 nm was measured [7], whereas tracks of 30-MeV C$_{60}$ cluster projectiles exhibited cross sections of varying shapes and with diameters between 8 and 16 nm [8]. In addition, ion-induced damage and correlated stress were studied by X-ray diffraction (XRD), also revealing an anisotropic response to the damage process [9].

Tracks annealed at elevated temperatures shrink in length and decay into damage segments interconnected by partially reconstructed lattice regions. Because the thermal history of geological samples has a significant impact on dating, extensive track annealing experiments have been performed under various temperature and time conditions. In contrast, the relevance of pressure on track formation is more difficult to access. Structural changes of pressurized non-irradiated apatite samples were examined with Raman spectroscopy displaying phase stability up to 25 GPa at room temperature (RT) [10]. Exposure to pressures above 12 GPa and simultaneously to temperatures up to 2300 °C created the γ-Ca$_3$(PO$_4$)$_2$ phase, which is stable only at high pressure [11].

The question of whether fission-track generation is possibly influenced by the presence of high pressure can now be tackled by laboratory radiation experiments. In a recent novel approach, pressure was included as a parameter by squeezing a small zircon sample between two diamond anvils at RT, and irradiating it with energetic ion projectiles. The simultaneous exposure to

✉ Fax: +86-931-8272100, E-mail: j.liu@impcas.ac.cn
*Present address: Department of Geological Sciences, University of Michigan, Ann Arbor, USA

a pressure of 14 GPa and to energetic U ions (24.5 keV/nm) was shown to trigger the transformation of zircon into its metastable phase reidite at a much lower pressure than without ion irradiation [12]. Tracks in zircon and their annealing behavior are also of interest for dating and have been examined systematically by XRD and Raman spectroscopy [13, 14].

In this study, the damage evolution in apatite was analyzed as a function of irradiation fluence and external pressure. We present new results based on Raman spectroscopy of single crystals that were ion irradiated at RT (1) in vacuum, (2) at ambient pressure, and (3) at simultaneous exposure to high pressure. The response of apatite to ion irradiation under external pressure is of interest not only in geosciences but also in materials science.

2   Experimental

As material we used several transparent, inclusion-free single crystals of Durango apatite from Mexico $(Ca_5(PO_4)_3(OH,F,Cl))$ of mass density ~ 3.2 g/cm^3 and hexagonal $P6_3/m$ structure. Prior to ion irradiation, all samples were annealed at $430\,^\circ$C for 24 h in order to eliminate existing tracks from spontaneous nuclear fission (samples prepared in this way are denoted throughout this paper as 'non-irradiated'). The irradiation experiments were performed at RT and under beam incidence normal to the c axis of the crystal. Irradiations without external pressure were carried at the UNILAC linear accelerator of GSI using U ions of 11.4 MeV/u. The initial beam energy is reduced to 11.1 MeV/u at the sample surface because the ions first passed through three aluminum foils (total thickness $\sim 3\,\mu$m) serving for fluence on-line control. The fluence applied varied between 1×10^{10} and 8×10^{12} ions/cm^2 (Table 1).
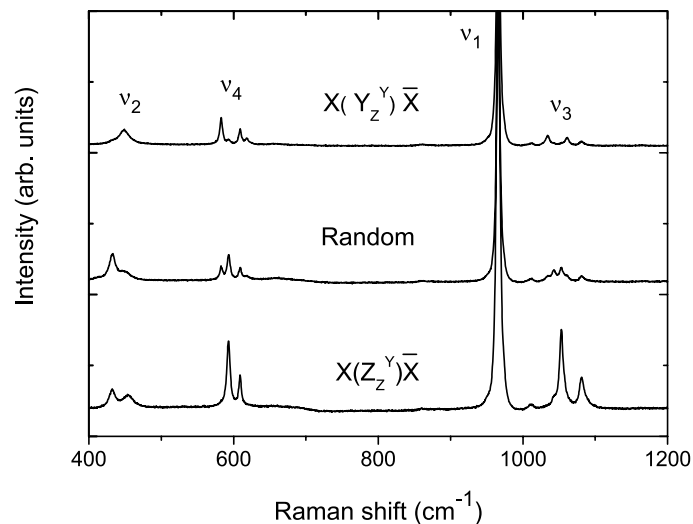
For the pressure experiment, a small-sized sample ($\sim 80\,\mu$m in diameter) was mounted in a Merrill–Bassett type diamond anvil cell (DAC). A 4 : 1 mixture of methanol and ethanol served as pressure-transmitting medium, and the pressure in the DAC was monitored via ruby fluorescence with an uncertainty of ~ 0.5 GPa. The sample pressurized to 10.5 GPa was irradiated with Kr ions of initial energy ~ 110 MeV/u available at the SIS heavy-ion synchrotron of GSI. The ions first passed through one of the two diamond anvils in which they slowed down from initially 8.9 GeV to about 2.1 GeV at the sample site. The fluence was 5×10^{11} ions/cm^2, and the energy loss of the projectiles when entering the sample amounted to ~ 6 keV/nm. Further information about the irradiation procedure is given in [12, 15]. As reference, a non-pressurized apatite sample mounted behind a single diamond anvil was irradiated in ambient air under the same fluence and energy loss conditions. Table 1 summarizes essential parameters of the irradiation experiments such as dE/dx and the projected ion range (R_p) as calculated with the computer code SRIM 2003 [16].

Before and after beam exposure, the samples were characterized by Raman spectroscopy with a Jobin-Yvon HR800 confocal spectrometer using the 632.8-nm line of a He–Ne laser in 180° backscattering geometry. To study the sample pressurized in the DAC, the incident 20-mW laser beam was focused with a long-working-distance $\times 50$ objective to a diameter of approximately $2\,\mu$m, whereas for the other samples a diameter of $\sim 1\,\mu$m was adjusted with a $\times 100$ objective. The scattered light was analyzed with a spectral precision of about 0.8 cm^{-1} using a grating of 1800 grooves mm^{-1}. We applied a notch holographic filter and recorded the photon intensity with an air-cooled CCD detector. Intensities, positions, and widths of the Raman resonances were determined by fitting Lorentzians to the peaks.

Ion	E_0 (GeV)	E_1 (GeV)	dE/dx (keV/nm)	R_p (μm)	Fluence (ions/cm^2)	Pressure
^{238}U	2.71	2.64	34	83	1×10^{10}	Vacuum
^{238}U	2.71	2.64	34	83	5×10^{10}	Vacuum
^{238}U	2.71	2.64	34	83	1×10^{11}	Vacuum
^{238}U	2.71	2.64	34	83	5×10^{11}	Vacuum
^{238}U	2.71	2.64	34	83	1×10^{12}	Vacuum
^{238}U	2.71	2.64	34	83	8×10^{12}	Vacuum
^{84}Kr	8.90	2.10	6	238	5×10^{11}	10.5 GPa
^{84}Kr	9.25	2.10	6	238	5×10^{11}	Ambient

TABLE 1   Compilation of essential irradiation parameters. E_0 denotes the initial kinetic energy of the ions as provided by the accelerator, E_1 and dE/dx are the energy and the electronic energy loss of the ions at the sample surface, and R_p is the projected ion range in apatite


FIGURE 1   Raman spectra of an annealed but non-irradiated natural apatite single crystal recorded for three different crystal orientations with respect to the incident linearly polarized laser beam. The different bands are assigned to modes of the phosphate group: ν_1 (symmetric stretching), ν_2 (symmetric bending), ν_3 (antisymmetric stretching), and ν_4 (antisymmetric bending)

3   Results and discussion

Before studying irradiated apatite, Raman spectra of non-irradiated samples were measured for calibration purposes in random and in $X(Y_Z^Y)\overline{X}$ and $X(Z_Z^Y)\overline{X}$ orientations. The expression $X(Y_Z^Y)\overline{X}$ denotes a geometry in which the incident laser beam is directed and the scattered light is recorded along the X and $\overline{X}$ axes of the crystal, respectively. The incident laser light was linearly polarized, with the electric field vector parallel to the Y axis. Figure 1 displays the three spectra and assignments of the PO_4 internal modes. In $X(Y_Z^Y)\overline{X}$ geometry, all A_g, E_{1g}, and E_{2g} Raman-active modes can be observed. In $X(Z_Z^Y)\overline{X}$ geometry, only the A_g and E_{1g} modes occur, while E_{2g} is forbidden. Raman-active vibrations can be attributed to the following phosphate modes: $964\,cm^{-1}$ to the ν_1 symmetric stretching vibration of phosphate anions, 430 and $453\,cm^{-1}$ to the ν_2 symmetric out-of-plane bending modes, 1052 and $1081\,cm^{-1}$ to the ν_3 antisymmetric stretching modes, and 591 and $608\,cm^{-1}$ to ν_4 antisymmetric bending [17–19]. All spectra presented in Sects. 3.1 and 3.2 were acquired in $X(Z_Z^Y)\overline{X}$ geometry.

3.1   *Irradiation of non-pressurized samples*

A series of apatite Raman spectra before and after the irradiation of single apatite crystals with U ions of various fluences (see Table 1) is shown in Fig. 2. The spectrum of non-irradiated apatite is dominated by the intense and relatively narrow $\nu_1(A_g)$ band centered at $964\,cm^{-1}$ and as-
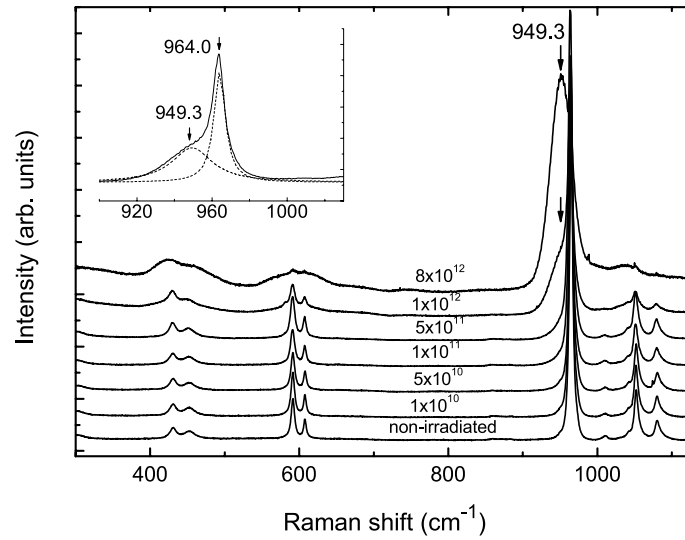
FIGURE 2   Raman spectra of a non-irradiated and of irradiated apatite samples. The irradiations were performed with 2.64-GeV U ions ($dE/dx = 34\,keV/nm$) at various fluences given in units of ions/cm². The *inset* shows the ν_1 mode splitting at fluence 1×10^{12} ions/cm². The linearly polarized laser light propagated normal to the crystallographic c axis, with the electric field vector oscillating parallel to this axis

signed to the Raman-active A_g mode. Further A_g resonances appear at 450, 608, 1052, and $1081\,cm^{-1}$. The E_{1g} mode is at 430 and $591\,cm^{-1}$. With increasing fluence, the positions, widths, and relative intensities of the different bands changed (Table 2). With respect to the non-irradiated sample, the changes are marginal for fluences up to 1×10^{11} ions/cm². Above this value, the bands broadened, the crystals were strained, and at 5×10^{11} ions/cm² cracked along planes normal to the c axes (see Fig. 3). A sample irradiated with a fluence of 8×10^{12} ions/cm² spontaneously decomposed into small pieces, but the remaining grains were still large enough to perform Raman spectroscopy.
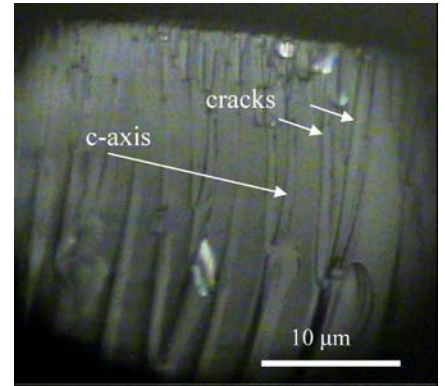
FIGURE 3   Optical micrograph of apatite sample irradiated with 2.64-GeV U ions of $dE/dx = 34\,keV/nm$ at a fluence of 5×10^{11} ions/cm². The beam incidence was normal to the surface. The *arrows* indicate cracks induced along the c plane

Ion	Pressure (GPa)	Fluence (ions/ cm²)	$\nu_{2b}(E_{1g})$ (430 cm⁻¹)			$\nu_{2b}(A_g)$ (453 cm⁻¹)			$\nu_{4b}(E_{1g}+A_g)$ (591 cm⁻¹)			$\nu_{4a}(A_g)$ (608 cm⁻¹)			$\nu_1(A_g)$ (964 cm⁻¹)			$\nu_{3b}A_g$ (1052 cm⁻¹)			$\nu_{3a}A_g$ (1081 cm⁻¹)		
			$\Delta\nu$ cm⁻¹	I/I_0 %	$\Delta\Gamma$ cm⁻¹	$\Delta\nu$ cm⁻¹	I/I_0 %	$\Delta\Gamma$ cm⁻¹	$\Delta\nu$ cm⁻¹	I/I_0 %	$\Delta\Gamma$ cm⁻¹	$\Delta\nu$ cm⁻¹	I/I_0 %	$\Delta\Gamma$ cm⁻¹	$\Delta\nu$ cm⁻¹	I/I_0 %	$\Delta\Gamma$ cm⁻¹	$\Delta\nu$ cm⁻¹	I/I_0 %	$\Delta\Gamma$ cm⁻¹	$\Delta\nu$ cm⁻¹	I/I_0 %	$\Delta\Gamma$ cm⁻¹
U	–	0	0	3.1	0	0	2.2	0	0	11.9	0	0	5.6	0	0	100	0	0	14.4	0	0	5.5	0
		1×10^{10}	−0.3	3.2	0.5	−0.2	2.3	−0.9	−0.1	12.7	0.2	−0.1	5.8	0.1	−0.2	100	0.2	−0.2	14.5	0.1	−0.2	5.7	0
		5×10^{10}	−0.1	3.3	0.7	0	2.1	−1.6	−0.1	11.5	0.5	0.1	5.5	0.3	0.1	100	0.1	0.1	13.5	0.2	0.2	5.2	0.2
		1×10^{11}	−0.5	3.3	1.2	−0.5	2.5	0.9	−0.4	11.5	1.2	−0.2	5.7	0.7	−0.8	100	0.7	−0.7	12.9	1.2	−0.6	5.2	0.2
		5×10^{11}	−0.7	4.0	1.5	−0.3	2.6	1.6	−0.4	12.5	1.4	−0.4	5.8	0.7	−0.9	100	1.2	−0.8	12.8	1.6	−1.0	5.3	−0.2
		1×10^{12}	−1.8	8.7	18.1	−2.9	3.8	2.3	−0.7	12.7	6.8	0.3	6.3	2.3	−1.4	100	2.5	−3.6	9.0	6.1	−1.3	5.7	2.5
Kr	–	0	0	3.1	0	0	2.2	0	0	11.9	0	0	5.6	0	0	100	0	0	14.4	0	0	5.5	0
	10.5	5×10^{11}	−0.4	4.9	2.0	−0.7	2.3	−0.5	−0.5	11.9	1.5	−0.3	4.6	1.1	−1.0	100	1.5	−1.1	11.8	3.4	−1.0	4.2	1.9
	–	5×10^{11}	−0.9	3.2	2.0	−1.4	2.7	3.5	−1.5	13.0	2.5	−1.4	6.0	1.3	−1.3	100	1.5	−0.8	13.7	1.9	−0.8	5.6	3.6

TABLE 2   Characteristics of phosphate Raman modes for different irradiation parameters. $\Delta\nu$ is the frequency shift of the band, $\Delta\Gamma$ is the change of width, and I/I_0 denotes the ratio of a given band peak intensity to the most dominant band $\nu_1(A_g)$ at $964\,cm^{-1}$ (symmetric stretching mode)
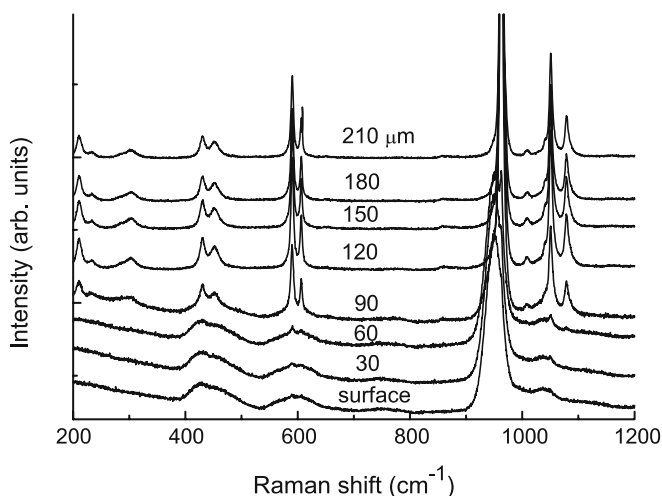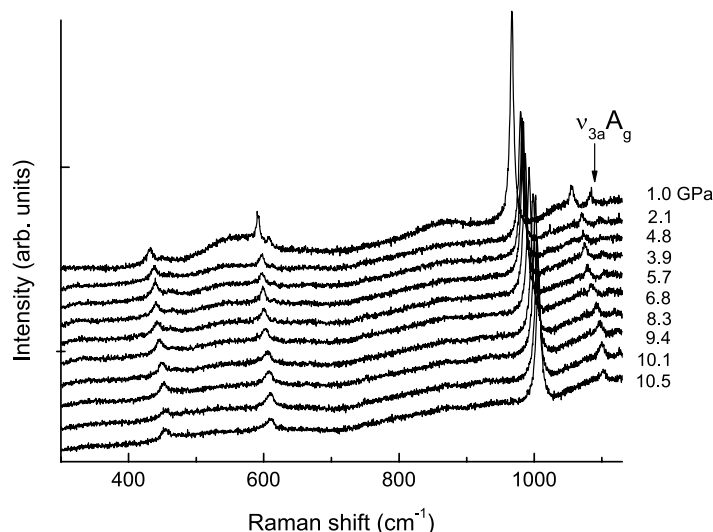
FIGURE 4 Raman spectra of apatite irradiated in vacuum with 2.64-GeV U ions of $dE/dx =$ 34 keV/nm at a fluence of 8×10^{12} ions/cm^2. The spectra were recorded successively by moving the laser focus from the surface into the bulk in steps of 30 μm per spectrum. Thus, the second spectrum is taken at 30-μm depth, the third at 60-μm depth, and so on. The respective nominal focus depth is assigned to each spectrum

FIGURE 5 Optical micrograph of sample pressurized in a diamond anvil cell to 10.5 GPa and irradiated with 2.1-GeV Kr ions ($dE/dx =$ 6 keV/nm) at a fluence of 5×10^{11} ions/cm^2. The two ruby crystals on the *right-hand side* serve for pressure calibration by fluorescence measurement

Compared to the non-irradiated sample, the position of the $v_{2b}(E_{1g})$ band shifted after the irradiation with 1×10^{12} ions/cm^2 from 430.7 to 428.9 cm^{-1} and its width increased from 10.1 to 28.2 cm^{-1}. The strong $v_1(A_g)$ peak at 964 cm^{-1} became weaker and broader, and the relative intensities of v_2, v_3, and v_4 with respect to v_1 grew with increasing ion fluence except for $v_{3b}(A_g)$. For instance, the relative intensity of the $v_{2b}(E_{1g})$ peak changed from 3.1 to 8.7% and for the $v_{2b}(A_g)$ peak from 2.2 to 3.8%.
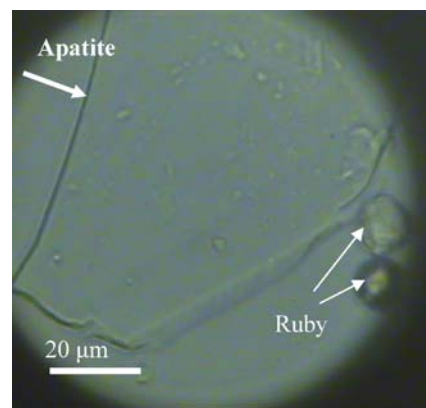
The spectrum of the sample exposed to 8×10^{12} ions/cm^2 exhibits only broad features; the previously separated and sharp modes have disappeared. We note that at a fluence of around 1×10^{12} ions/cm^2, a new $v_1(A_g)$ peak ascribed to phonons emerges at 949 cm^{-1} (see inset in Fig. 2), becoming pronounced at 8×10^{12} ions/cm^2. The decrease of symmetric vibration modes is ascribed to increasing amorphization and thus distortion of the PO$_4^{3-}$ tetrahedra. Assuming cylindrical amorphous tracks of diameter 10 nm, the contribution of amorphized material in the irradiated layer of our samples is estimated to be $\sim 30\%$ for 5×10^{11} ions/cm^2. The amorphous fraction increases to $\sim 50\%$ for 1×10^{12} ions/cm^2 and, finally, the entire sample is expected to be amorphized at 8×10^{12} ions/cm^2.

Figure 4 displays Raman spectra of a sample irradiated at the UNILAC with 2.64-GeV U ions of fluence 8×10^{12} ions/cm^2. The spectra were recorded successively by changing the distance between sample surface and spectrometer objective in steps of 30 μm per spectrum. The first four spectra down to a nominal depth of 90 μm are similar to each other and differ significantly from the data recorded from deeper layers. The spectra were acquired without immersion liquid and thus the absolute depth of the focal plane is not well defined. However, within the given accuracy, the two different signals can be assigned to the irradiated surface layer and to the non-irradiated substrate layer, respectively, indicating that the

sample crystallinity was changed within but remained unchanged beyond the ion range.

3.2   *Irradiation under high pressure*

A photograph of the small-sized apatite sample mounted in the DAC and pressurized to 10.5 GPa is shown in Fig. 5. After irradiation with Kr ions of fluence 5×10^{11} ion/cm^{-2} (Table 1), Raman spectroscopy of the pressurized sample was performed through the diamond of the DAC while releasing the pressure step by step to ambient conditions (Fig. 6). With decreasing pressure, all bands shift to

FIGURE 6 Raman spectra of apatite sample irradiated at 10.5 GPa with 2.1-GeV Kr ions of $dE/dx = 6$ keV/nm at a fluence of 5×10^{11} ions/cm^2. The spectra of the sample mounted in the DAC were recorded through one of the diamond anvils while releasing the pressure step by step

smaller wavenumbers (see Table 2), e.g. the peak position of the $\nu_1(A_g)$ mode shifts from $1006\,\mathrm{cm}^{-1}$ at 10.5 GPa to $964\,\mathrm{cm}^{-1}$ at ambient pressure. At 3.9 GPa, the second component of the $\nu_{3a}(A_g)$ antisymmetric stretching mode appears at $1081\,\mathrm{cm}^{-1}$. For the Raman bands at 1052, 964, 591, and $430\,\mathrm{cm}^{-1}$, the peak shifts with decreasing pressure are plotted in Fig. 7. Based on these results, the dimensionless Grüneisen parameter γ_i of each mode was calculated by applying the equation

$$\gamma_i = \left(\frac{\delta\nu_i}{\delta P}\right)\frac{K}{\nu_i},$$

where ν_i and $\delta\nu_i$ denote respectively the frequency and frequency shift of mode i, δP is the pressure change, and K is the bulk elasticity modulus amounting to 93 GPa for apatite. The Grüneisen parameter describes the alteration of the vibration frequency in a crystal lattice due to increased or decreased lattice volume resulting from temperature or pressure changes. Using the slopes of the curves in Fig. 7, the γ values of the $\nu_{2b}(E_{1g})$, $\nu_{4b}(E_{1g} + A_g)$, $\nu_1(A_g)$, and $\nu_{3b}(A_g)$ Raman bands were calculated to be respectively 0.53, 0.34, 0.40, and 0.44, in agreement with results reported in the literature for phosphate modes of non-irradiated apatite [20].

In contrast to the sample irradiated at the UNILAC, none of the samples exposed to the higher energies exhibited cracks. This difference is ascribed to the fact that the UNILAC ions penetrate only about 80 μm into the crystal and thus amorphize only a thin surface layer of the thick crystal, whereas the SIS ions have sufficiently high energy to pass completely through the sample.

Figure 8 depicts Raman spectra of a non-irradiated sample and of two samples irradiated with $5 \times 10^{11}\,\mathrm{cm}^{-2}$ Kr ions of 2.1 GeV. One of the samples was pressurized to 10.5 GPa during the irradiation; the other was exposed under the same conditions but at ambient pressure. The peak intensity ratio of $\nu_{2b}(A_g)$ and $\nu_1(A_g)$ is 2.7, 2.3, and 2.2 for the non-irradiated sample and for the samples irradiated at 10.5 GPa and at ambient conditions, respectively. Compared to the non-irradiated sample, the peak positions of the irradiated samples are shifted by $-0.7\,\mathrm{cm}^{-1}$ (irradiated at 10.5 GPa) and by $-1.4\,\mathrm{cm}^{-1}$
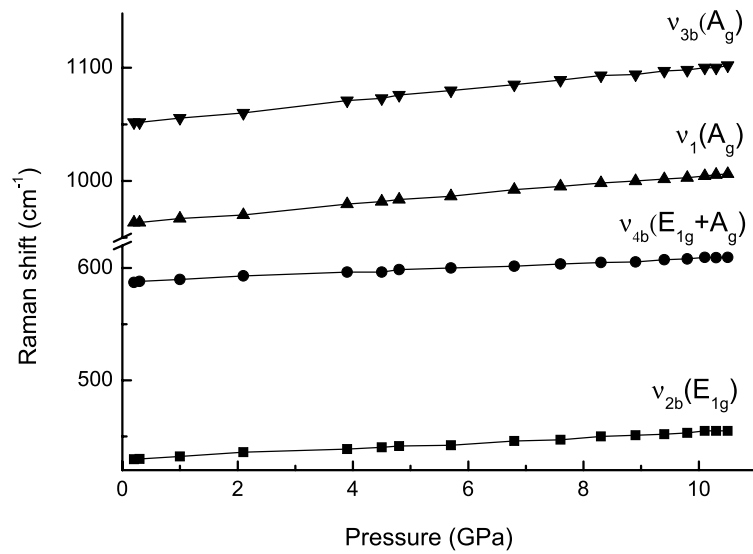

FIGURE 7 Positions of band maxima of the phosphate modes as a function of pressure deduced from Raman spectra shown in Fig. 6
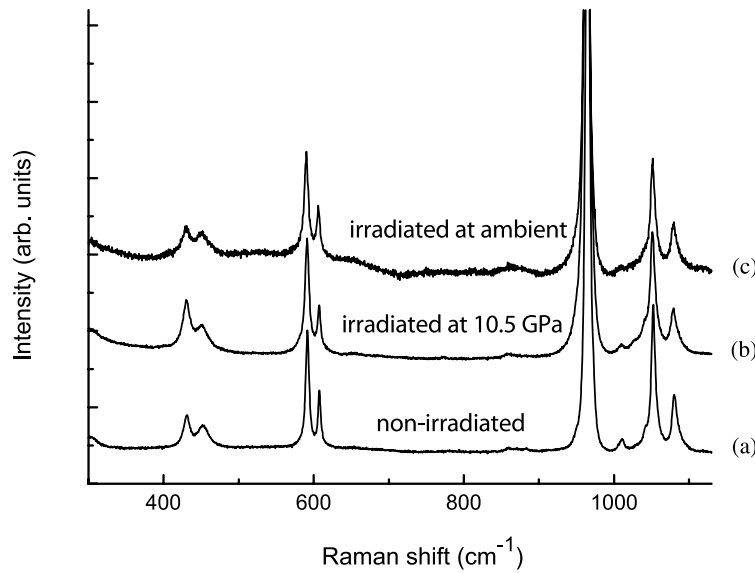

FIGURE 8 Raman spectra of (a) non-irradiated apatite and of samples irradiated with 2.1-GeV Kr ions of fluence 5×10^{11} ions/cm^2: (b) under pressure of 10.5 GPa and (c) under ambient conditions. The Raman spectrum of (b) was recorded after pressure release

(irradiated at ambient conditions), indicating that beam exposure at ambient conditions causes more damage than under elevated pressure. It seems that the pressure strengthens the crystal lattice against damage from heavy-ion irradiation.

4 Conclusion

In summary, the analysis of Raman spectra demonstrates that apatite single crystals irradiated with swift heavy ions undergo structural changes. The effect is ascribed to the creation of amorphous tracks embedded in the crystalline matrix. The change of the vibrational modes is marginal at fluences below 5×10^{11} ions/cm^2, but becomes considerable when increasing the fluence to 8×10^{12} ions/cm^2. Concomitant significant strain is induced causing cracking and finally breakage of the crystal. This effect is in particularly strong in samples exposed to 2.7-GeV U ions, which are stopped at a depth of ~ 80 μm and thus induce amorphization only in the thin irradiated surface layer on top of the underlying crystal. Comparing the Raman spectrum of the sample irradiated at 10.5 GPa with the one exposed to an ion beam with the same

parameters, but under ambient conditions, shows that fewer modifications are induced. This suggests that pressure increases the radiation stability of the lattice. This finding has to be examined by more systematic irradiation experiments at different pressures and using several ion species and fluences.

REFERENCES

1 G.A. Wagner, E. Hejl, Chem. Geol. **87**, 1 (1991)
2 C. Hepburn, A.H. Windle, J. Mater. Sci. **15**, 279 (1980)
3 J.Y. Kim, Z.L. Dong, T.J. White, J. Am. Ceram. Soc. **88**, 1253 (2005)
4 F. Villa, M. Grivet, M. Rebetez, C. Dubois, A. Chambaudet, N. Chevarier, G. Blondiaux, T. Sauvage, M. Toulemonde, Nucl. Instrum. Methods B **72**, 168 (2000)
5 M. Grivet, M. Rebetez, A. Chambaudet, N. Ben Ghouma, Nucl. Tracks Radiat. Meas. **22**, 779 (1993)
6 T.A. Paul, P.G. Fitzgerald, Am. Mineral. **77**, 336 (1992)
7 M. Lang, Doctoral thesis, University of Heidelberg (2004)
8 G. Jaskierowicz, A. Dunlop, R. Jonckheere, Nucl. Instrum. Methods B **222**, 213 (2004)
9 S. Miro, D. Grebille, D. Chateigner, D. Pelloquin, J.P. Stoquert, J.J. Grob, J.M. Costantini, F. Studer, Nucl. Instrum. Methods B **227**, 306 (2005)
10 Q. Williams, E. Knittle, J. Phys. Chem. Solids **57**, 417 (1996)
11 J.K. Murayama, M. Kato, S. Nakai, M. Kumazawa, Phys. Earth Planet. Interiors **44**, 293 (1986)
12 U.A. Glasmacher, M. Lang, H. Keppler, F. Langenhorst, R. Neumann, D. Schardt, C. Trautmann, G.A. Wagner, Phys. Rev. Lett. **96**, 195701 (2006)
13 L. Nasdala, P.W. Reiners, J.I. Garver, A.K. Kennedy, R.A. Stern, E. Balan, R. Wirth, Am. Mineral. **89**, 219 (2004)
14 L. Nasdala, C.L. Lengauer, J.M. Hanchar, A. Kronz, R. Wirth, P. Blanc, A.K. Kennedy, A.-M. Seydoux-Guillaume, Chem. Geol. **191**, 121 (2002)
15 M. Lang, U.A. Glasmacher, R. Neumann, D. Schardt, C. Trautmann, G.A. Wagner, Appl. Phys. A **80**, 691 (2005)
16 J. Ziegler, J. Biersack, D. Marwick, *SRIM-2003: The Stopping and Range of Ions in Matter* (IBM, New York, 2000)
17 L.C. Kravitz, J.D. Kingsley, E.L. Elkin, J. Chem. Phys. **49**, 4600 (1968)
18 L.L. Boyer, P.A. Fleury, Phys. Rev. B **9**, 2693 (1974)
19 M. Zattin, D. Bersani, A. Carter, Chem. Geol. **240**, 197 (2007)
20 P. Comodi, Y. Liu, M.L. Frezzotti, Phys. Chem. Mineral. **28**, 225 (2001)